

# A Method to Quantify Vehicle Dynamics and Deformation for Vehicle Rollover Tests Using Camera-Matching Video Analysis

**Nathan A. Rose**  
**William T.C. Neale**  
**Stephen J. Fenton**  
**David Hessel**  
Kineticorp, LLC

**Robert W. McCoy**  
Ford Motor Company

**Clifford C. Chou**  
Wayne State University

Copyright © 2008 SAE International

## ABSTRACT

This paper examines the use of camera-matching video analysis techniques to quantify the vehicle dynamics and deformation for a dolly rollover test run in accordance with the SAE Recommended Practice J2114. The method presented enables vehicle motion data and deformation measurements to be obtained without the use of the automated target tracking employed by existing motion tracking systems. Since it does not rely on this automated target tracking, the method can be used to analyze video from rollover tests which were not setup in accordance with the requirements of these automated motion tracking systems. The method also provides a straightforward technique for relating the motion of points on the test vehicle to the motion of the vehicle's center-of-mass.

This paper, first, describes the specific rollover test that was utilized. Then, the camera-matching method that was used to obtain the vehicle motion data and deformation measurements is described. Finally, the data obtained from the video analysis is analyzed and compared to data obtained from on-board instrumentation. Ultimately, the camera-matching technique is shown to be a viable technique for obtaining three-dimensional vehicle motion during a rollover crash test. As a means of obtaining vehicle deformation, the technique will need further development.

## INTRODUCTION

This paper examines the use of a camera-matching photogrammetric technique to track the motion and dynamic deformation of a vehicle during a SAE J2114 dolly rollover test. The methodology presented enables vehicle motion data and deformation measurements to be obtained without the use of the automated target tracking employed by motion tracking systems. Since it does not rely on this automated target tracking, the method can be used to analyze video from rollover tests which were not setup in accordance with the requirements of such motion tracking systems. The method also provides a straightforward technique for relating the motion of points on the test vehicle to the motion of the vehicle's center-of-mass.

In 2006, Chou, et al. (2006), reported video analysis results for a 500 millisecond segment of another dolly rollover test [1]. In this earlier research, the authors primarily examined the effectiveness of the technique for obtaining roll angles and roll velocities from the test. The analysis reported by Chou, et al., was limited because the characteristics and locations of the cameras that recorded the crash test were unknown, as was the exact geometry of the crash test facility and the crash test vehicle.

This paper reports data and results from a more extensive analysis of a dolly rollover test. In this study, the geometry of the crash test facility and the locations and characteristics of the cameras that recorded the test were surveyed and documented. Knowledge of the camera characteristics enabled better modeling of the cameras in a three-dimensional computer environment than what was possible in the previous analysis by Chou, et al (2006). Also, it enabled correction of the crash test video for lens distortion. In addition, a number of targets were placed on the crash test vehicle and the vehicle geometry and target locations relative to this geometry were surveyed. More detailed documentation of the vehicle geometry enabled more precise matching of the vehicle motion visible in the video. The analysis reported here included a 2000 ms segment of the test and yielded motion data that included the x, y and z position and the roll, pitch and yaw angles for the vehicle throughout that time period. Based on this motion data and on knowledge of the vehicle and crash test facility geometries, translational and angular velocities, accelerations and deformations for the test vehicle were also obtained.

In this paper, we first describe the parameters of the rollover test that was utilized for this video analysis. Then, the camera-matching method that was used to obtain the vehicle motion and deformation is described. Finally, the data obtained from the video analysis is analyzed and then compared to data obtained from on-board instrumentation.

## **ROLLOVER TEST SETUP**

The motion analysis reported in this paper used a laboratory-based J2114 dolly rollover test [2, 3] which was run with a Ford sport utility vehicle. The test vehicle is shown in Figure 1.



**Figure 1 – Test Vehicle**

This vehicle was instrumented with sensors to measure the vehicle-fixed longitudinal, lateral and vertical accelerations at the center tunnel between the seats and

the lateral and vertical accelerations at the lower A-pillar on both sides of the vehicle. Based on the axle weights of the test vehicle, the sensors mounted on the center tunnel between the seats were near the longitudinal position of the vehicle's center-of-mass. The vehicle was also instrumented with two angular rate sensors for each principal axis. These were mounted on the center tunnel just rearward of the seats. Nine high-speed, stationary cameras and one real-time panning camera recorded the test. The high-speed video was taken at 500 frames per second and the real-time video was taken at the NTSC standard frame rate of 29.97 frames per second.

Prior to the test, a number of targets, which are visible in Figure 1, were placed on the vehicle and their locations were surveyed. The overall geometry of the vehicle was also surveyed. In addition, features of the crash test facility geometry that would be visible in the crash test video were surveyed. Similar surveys of the vehicle and crash test geometries were later conducted after the test. These post-test surveys included physical evidence deposited by the vehicle on the test surface.

The rollover dynamics that occurred during the test are depicted in Figure 2, which contains a series of images that were captured by one of the high-speed cameras located downstream of the roll. As these images show, the vehicle rolled just past 360 degrees and then reversed its roll direction and came to rest on its wheels.

## **CAMERA-MATCHING VIDEO ANALYSIS**

### **METHODOLOGY**

This section describes the methodology utilized to track the vehicle motion in the crash test video. This methodology consisted of the following steps: 1) preparing the test vehicle with targets that would be tracked; 2) surveying the test facility and vehicle geometries; 3) creating a computer environment that included the geometries of the test facility and the test vehicle; 4) analyzing the actual cameras and the video images to determine characteristics, distortion and resolution so that these could be replicated with computer-modeled cameras; 5) accurately placing computer-modeled cameras in a three-dimensional computer environment and matching them to the test video; and 6) tracking the movement of the test vehicle by matching the location of the computer generated vehicle targets to the targets on the test vehicle for each frame of the video sequence. These steps are detailed in the following subsections.

### **Preparation for Motion Tracking**

Prior to running the crash test, the test vehicle was marked with high-contrast yellow and black fiducial targets. It was the motion of these targets that was ultimately tracked in the video. In placing these targets,

the primary goal was to generate a wide range of points on the vehicle that would be visible and identifiable in the crash test video. Once these stickers were placed, their locations were surveyed so that they could be replicated on a computer-generated model of the test vehicle.

Also prior to running the crash test, 12-inch wide foam fiducial blocks were placed along the anticipated rollover path. These blocks were evenly spaced on both sides of

the roll path and were visible in at least one camera at all times during the rollover sequence. After placing these foam blocks, a survey of the test facility was completed. This survey provided the three-dimensional geometry of the rollover test facility, including the ground surface, the control joints in the concrete of the test surface, the walls surrounding the test surface, the light fixtures located above the test surface, and the foam fiducial blocks. This survey data provided the foundation for a computer model of the entire test area.

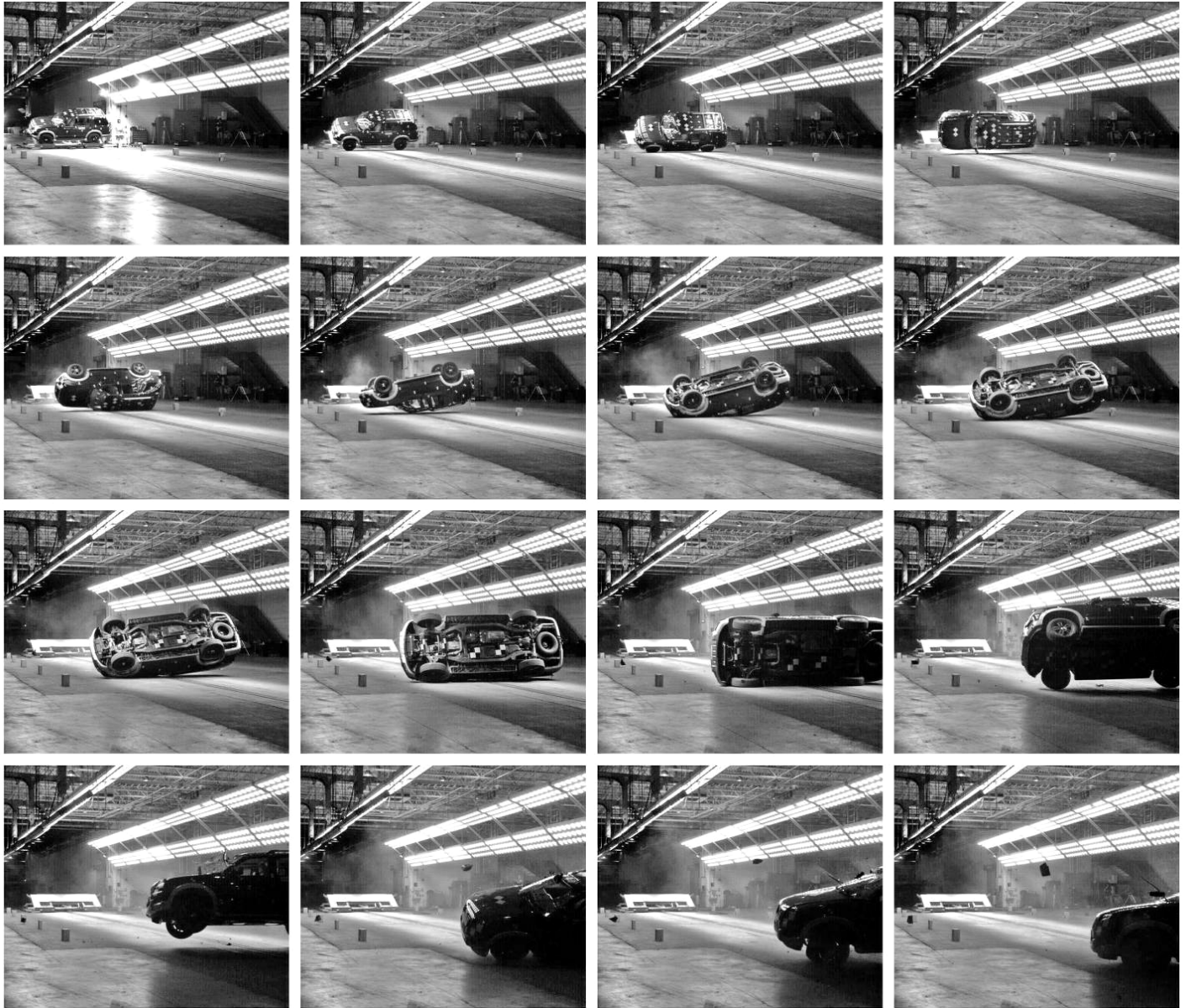


**Figure 2 – Rollover Dynamics for the Test**

### **Creation of the Computer-Modeled Environment**

Prior to the test, the crash test facility was surveyed using Sokkia Laser Survey equipment. This raw data was processed and through analysis of photos and other inspection notes, a computer-generated model of the

test facility was constructed using modeling programs such as Carlson, AutoCAD 2008, and MAX 8. The geometry included the concrete block sections of the rollover facility floor, the control joints that separate these blocks, CMU walls that surround the rollover area and the lights above the rollover area. This geometry

was constructed in the computer modeling programs and the entire computer environment was then oriented relative to the general roll direction. In addition, markers locating the position and orientation of the camera were also identified from the survey data and used as position markers for computer-modeled cameras that were later incorporated into the scene.

A detailed computer model of the test vehicle was obtained from an online model library. The accuracy of this model was verified through comparison to the data from our pre-test survey of the actual vehicle. With the survey of the test vehicle aligned to the computer model, the target stickers that were placed on the test vehicle, and subsequently surveyed, could be transferred to identical locations on the computer model of the vehicle. These target locations were used to track the motion of the test vehicle.

### Camera Characteristics and Specifications

In addition to creating a computer-modeled environment of the physical geometry of the facility, the optical and geometric characteristics of all the cameras were documented and analyzed in order to create computer-generated cameras that mimic each individual camera that captured video of the rollover test. The data for these cameras came from the survey of these cameras, analysis of the sensors, and analysis of the technical and specification drawings. Each camera was created

according to its specific characteristics, since these characteristics differed between cameras. These computer-modeled cameras were also located and oriented to be identical to the cameras surveyed at the facility at the time the dolly rollover test was conducted.

The high-speed cameras used for recording the rollover test were Redlake MotionXtra HG-LE digital video cameras. These cameras recorded the test at 500 frames per second with a maximum resolution of 752x1128 pixels and a pixel aspect ratio of 1.0. Figure 3 depicts the location of each camera relative to the test area and reports each camera's lens type and focal length and the image resolution with which each camera recorded the test. In the course of our pre-test documentation, the horizontal and vertical orientation of each of these cameras was documented using the laser survey equipment. When computer-modeled cameras were created for our video analysis, the camera characteristics reported in Figure 3 were replicated. The camera locations and orientations relative to the test area were also replicated when the computer-modeled cameras were setup within a three-dimensional computer model of the crash test facility. In addition to replicating the basic characteristics, locations and orientations of the actual cameras, the computer-modeled cameras used in the motion tracking analysis also utilized an accurately placed picture plane, which is the plane on which the camera lens focuses light and the plane on which the image sensors that record the digital image are located.

Location	Camera Number	Camera Type	Lens Type	Focal Length	Image Resolution
1	75	Redlake HG-LE	Pentax TV Lens	12.5mm	752x1128 pixels
2	55	Redlake HG-LE	Pentax TV Lens	12.5mm	752x1128 pixels
3	63	Redlake HG-LE	Tamaron	18mm	752x640 pixels
4	78	Redlake HG-LE	Schnick Kreuznach	20mm	752x640 pixels
5	94	Redlake HG-LE	Tamaron	18mm	752x640 pixels
6	52	Redlake HG-LE	Pentax TV Lens	12.5mm	752x1128 pixels
7	60	Redlake HG-LE	Kinoptik	45.6mm	752x640 pixels
8	64	Redlake HG-LE	Pentax TV Lens	12.5mm	752x1128 pixels
9	53	Redlake HG-LE	Schnick Kreuznach	20mm	752x640 pixels

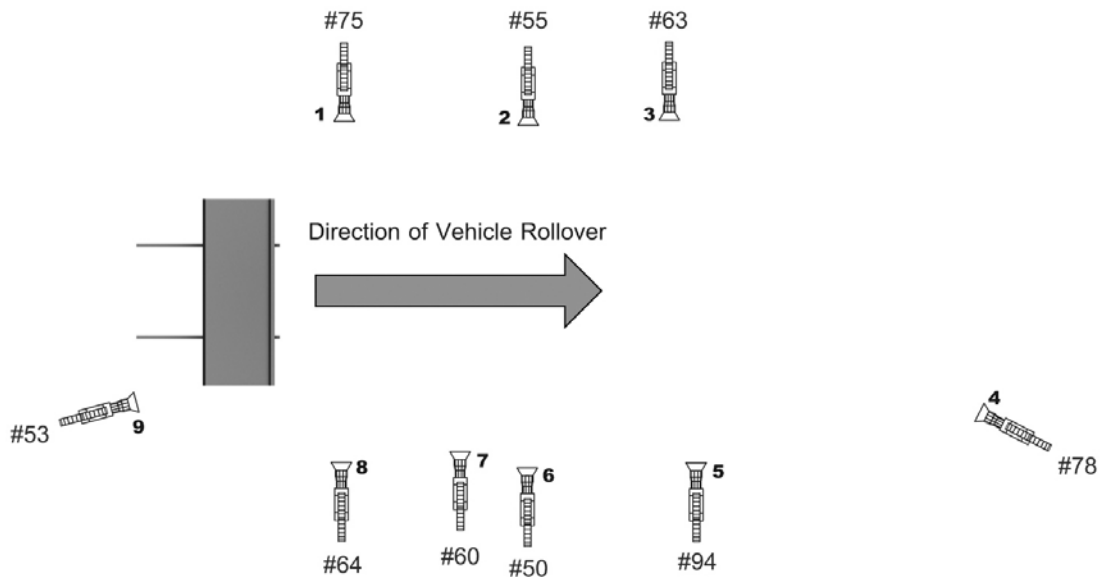


Figure 3 – Location and Characteristics of the Cameras

The image sensors in the digital cameras used to record this test were Complimentary Metal Oxide Semi-Conductor (CMOS) sensors with a 1504x1128 maximum pixel image resolution. This configuration yields a 1.7 megapixel video resolution. However, since this sensor is not a Charged Coupled Device (CCD) it tends to have a larger image resolution at the expense of light sensitivity. This characteristic means that when the test vehicle exits the lighted area (approximately 2 seconds after leaving the dolly), it becomes more difficult to identify the fiducial targets on the vehicle and hence the fidelity of the motion tracking in the dark area is reduced. For this reason, the motion of the vehicle was not tracked once it exited the lighted area of the test surface.

Another characteristic of the image sensors used in these cameras is that they have a four quadrant assembly with each quadrant containing one photodiode as shown in Figure 4.

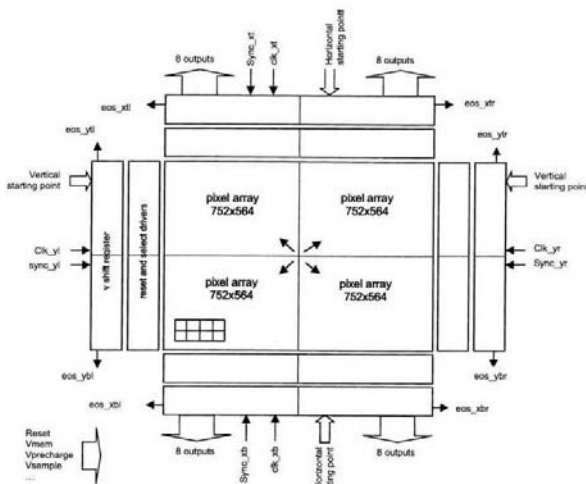


Figure 4 – Image Sensor

This configuration is useful for producing multiple sensor size configurations for various industries or consumers without having to change the sensor architecture. For example, 1, 2 or 4 quadrants could be active producing varying image resolutions. Because the configurations of the image sensor assembly differ it was relevant to analyze which configuration was used in the cameras in this test so the appropriate aperture width, which is determined by the sensor size, could be established for the computer-modeled cameras used in the video analysis.

Ultimately, it was determined that there were two different image sensor configurations in use during this test. Both configurations used quadrants one and four, though their pixel resolutions were different. For the cameras utilizing the full capabilities of the image sensors, the one and four quadrant sensor resulted in an image size of 752x1128. For the cameras that utilized only a portion of the available sensor image of quadrants one and four, a resolution of 640x752 resulted. This configuration produced two different image aspect ratios. The larger image had an image aspect ratio of 1.5. The active quadrants were areas 1 and 4 producing an image size of 752x1128. The smaller image produced an image aspect ratio of 1.175, and a resolution of 752x640 pixels. The difference between these resolutions can be seen in a frame captured from each camera shown in Figure 5.

For the Redlake CMOS sensors, 1 pixel of the image sensor measures  $12 \times 12 \mu\text{m}^2$ , and hence the camera aperture width for each of the actual cameras was 9.0mm. This aperture width was used in creating the computer-modeled cameras used for the video analysis. Figure 6 depicts examples of two of the computer-modeled cameras used in the analysis.



1128x752 pixel resolution (1.5 Image Aspect Ratio)



752x640 pixel resolution (1.175 Image Aspect Ratio)

Figure 5 – Frames Captured from Two High-Speed Cameras Used to Record the Test

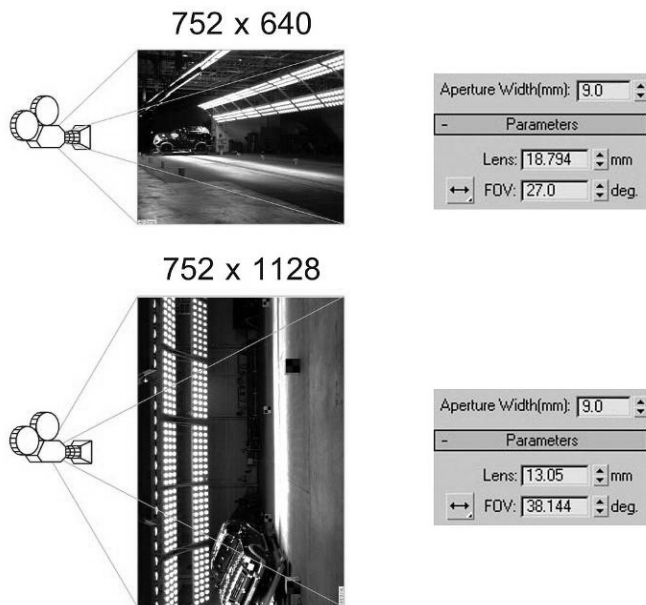


**Figure 6 – Computer-Modeled Camera Characteristics**

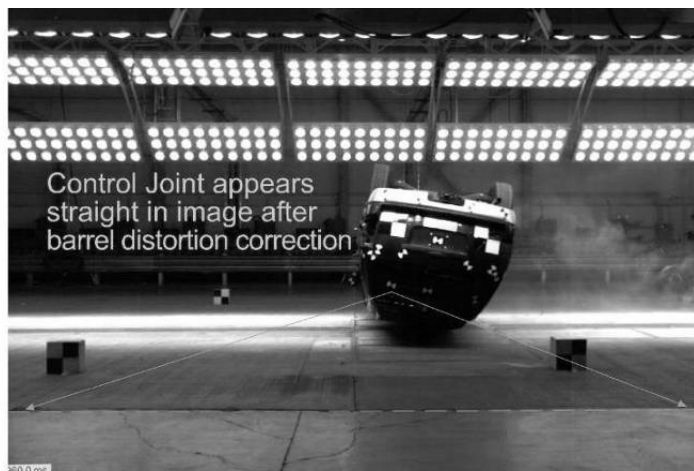
Lens distortion was visible in the test video, and therefore, needed to be accounted for in the camera-matching analysis. Lens distortion occurs in two basic forms, barreling and pin cushioning. Barreling and pin cushioning are opposite effects that distort the image by squashing or stretching the edges of the image, respectively. In general, barreling occurs from wide focal lengths while pin cushioning occurs from zoom focal lengths.

As demonstrated in Figure 7, there existed some barreling of the images as a result of lens distortion inherent in the camera lens focal length. An example of the barreling effect can be seen in the lower portion of the left image of Figure 7 where a concrete control joint on the floor of the test facility can be seen to curve up at both ends. As a result of this distortion, objects on the edges of the image appear squashed and if used in a video analysis would yield distances shorter than the actual distance.

Video compositing and editing software was used to eliminate the distortion from each video frame that was used for the motion tracking. Because barrel distortion is dependent on the camera system and the lens and focal length, analysis was performed on each video sequence to see if a different distortion correction was needed for each sequence. Due to the difference in focal length and in unique aspects of lens manufacturing, each lens ultimately required its own distortion correction.



Unrectified Image



Rectified Image

**Figure 7 – Lens Distortion Correction**

### Tracking the Vehicle Motion

Having created a computer-modeled environment that contained the geometry of the test facility, the test vehicle and a series of computer-modeled cameras that replicate the actual cameras, test video from each camera was then designated as a background image for its corresponding computer-modeled camera. For

instance, the first two cameras in line with the rollover sequence face each other and lay perpendicular to the roll path. Identified as Cameras #75 and #64 in Figure 3, these cameras were associated with video sequences obtained from that location and given the same name such as “camera#75.avi” and “camera#64.avi”, respectively. At this point, each computer-modeled camera could be used to simultaneously view the

computer model of the test facility and the crash test video. If the location and characteristics of each camera were set properly, then this step would yield an overlay between the video background and the computer-modeled environment. Crash test facility features visible in computer model should overlay those same features visible in the crash test video. Figure 8 depicts this process of camera-matching the computer-modeled cameras to the video of the rollover test.

This step was repeated for each camera position and video sequence, such that all cameras and computer geometry were visually determined to be matched to their background video sequence. With this determination, the computer model of the test vehicle could be placed in the computer-modeled environment and positioned at each frame to mimic the movements of the vehicle visible in each frame of the video sequence. Each camera was independently matched to the background, but there is only one vehicle model being matched in the environment. As a result, each view

helped to refine the position of the vehicle at each frame since the vehicle position could be viewed from several cameras at once.

The images in Figure 9 depict a properly matched computer model of the vehicle and facility for several frames of the video. The mesh model of the vehicle contains yellow dots as seen in the video image overlay. These yellow dots are the surveyed points of the test vehicle before it was damaged from the rollover. It can be seen in Figure 9 that these images match with all the corresponding targets that were placed on the test vehicle. In addition to the vehicle matching the video, the computer model of the environment and background can also be seen in this image properly oriented and positioned relative to the same background and environment of the facility seen in the video. After such a match was obtained for each video frame, position and orientation data for the vehicle in each frame could be exported for analysis in Microsoft Excel.

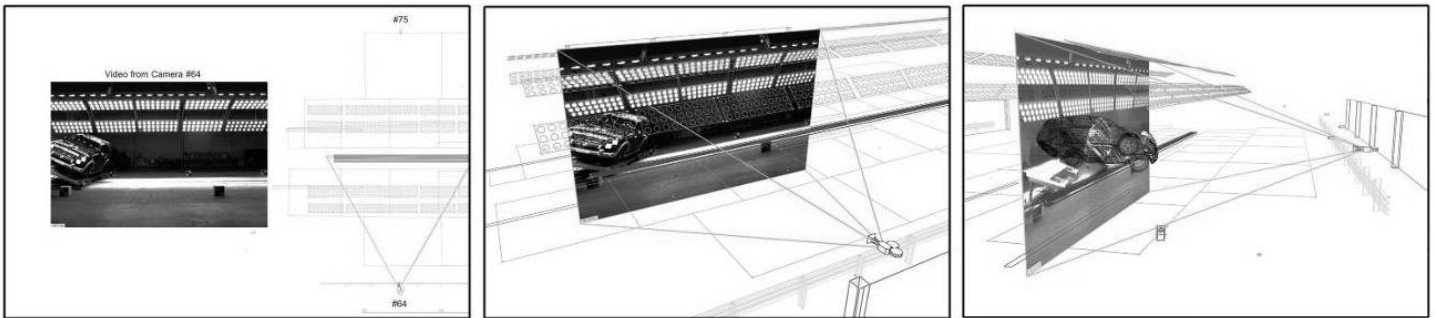


**Figure 8 – Camera-Matching Process**



**Figure 9 – Frames from Camera-Matched Video**

## MOTION ANALYSIS

The video analysis described in the previous sections yielded the earth-fixed x, y, and z coordinates of the vehicle center-of-mass (CoM) and the yaw, pitch and roll angles of the vehicle at 10 millisecond intervals throughout the first 2 seconds of the test. For the analysis presented here, the earth-fixed coordinate system was setup with the positive x direction running directly opposite the initial travel direction of the rollover dolly and the test vehicle. The positive y direction was oriented along the initial heading direction of the vehicle and the positive z axis was oriented upward.

Once the vehicle's positions and orientations were obtained, they were used to calculate the velocities and accelerations for the vehicle during the test. For instance, the following centered difference equation was used to obtain the vehicle's ground plane velocity throughout the test [5]:

$$v_{x-y} = \frac{\sqrt{(x_{t+\Delta t} - x_{t-\Delta t})^2 + (y_{t+\Delta t} - y_{t-\Delta t})^2}}{2\Delta t} \quad (1)$$

In this equation, x and y refer to the x and y coordinates of the vehicle's CoM, the subscripts t+Δt and t-Δt reference these coordinate values from time steps surrounding the time step of interest, and Δt is the duration of each time step.

Overall, it was found that the motion of the vehicle in the y-direction was negligible, such that the velocity of the vehicle in the x-direction (along the rollover track) was nearly identical in magnitude to the overall translational speed of the vehicle given by Equation (1). This x-direction velocity was obtained with the following equation:

$$v_x = \frac{x_{t+\Delta t} - x_{t-\Delta t}}{2\Delta t} \quad (2)$$

Similarly, the following centered difference equation was used to obtain the vehicle's vertical velocity throughout the test:

$$v_z = \frac{z_{t+\Delta t} - z_{t-\Delta t}}{2\Delta t} \quad (3)$$

In this equation, z refers to the z-coordinate of the vehicle's CoM.

In general, the accuracy and precision of the velocities calculated with Equations (1), (2) and (3) will depend on the magnitude of the measurement error in the positional coordinates and on the time step used for the calculation. On the one hand, if too small a time step is

used, the velocity calculations will be excessively sensitive to any measurement errors and will exhibit excessive uncertainty. On the other hand, if too large a time step is used, the velocity curves will suffer from over-smoothing error and the velocity peaks could be truncated [4].

To explore the degree to which measurement errors might affect the accuracy and the precision of the velocities calculated with Equations (2) and (3), the authors had a second analyst use the camera-matching technique to obtain a second set of motion for the vehicle in the first two seconds of the test, at time increments of 30 milliseconds. The positions and orientations of the vehicle obtained with this second analysis were then compared to the positions and orientations of the vehicle obtained by the first analyst. Overall, the two sets of motion data had an average difference in the x-coordinate of 0.35 inches, with a standard deviation of 0.36 inches, and an average difference in the z-coordinate of 0.42 inches, with a standard deviation of 0.28 inches. Thus, 84% of the time, the difference between the two analysts' positions was less than 0.71 inches. Around 96% of the time, the difference between the two analysts' positions was less than 1.0 inch.

Using differential calculus to perform an error analysis [8], it can be shown that the uncertainty in the velocities of Equations (2) and (3) can be estimated with the following equations:

$$\delta v_x = \frac{\delta x}{\sqrt{2} \cdot \Delta t} \quad (4)$$

$$\delta v_z = \frac{\delta z}{\sqrt{2} \cdot \Delta t} \quad (5)$$

In these equations, δx and δz are the positional uncertainties in the x and z coordinate directions and δv<sub>x</sub> and δv<sub>z</sub> are the velocity uncertainties in these same directions. In formulating Equations (4) and (5), it has been assumed that the potential measurement error at each time step is independent of those at the surrounding time steps.

Assuming that the differences between the two analysts reported above give us a reasonable estimate of the uncertainty in the positional coordinates obtained with the camera-matching technique, Figure 10 graphically represents the uncertainty in the translational velocities for time steps varying between 10 and 50 milliseconds. Figure 10 contains curves for an 84% confidence interval and a 96% confidence interval. As one would expect, the uncertainty in the velocities due to potential measurement errors decrease as the time step increases. A time step of 40 milliseconds produced an

uncertainty of 1 mph in the ground plane and vertical speeds, with a confidence of 96%.

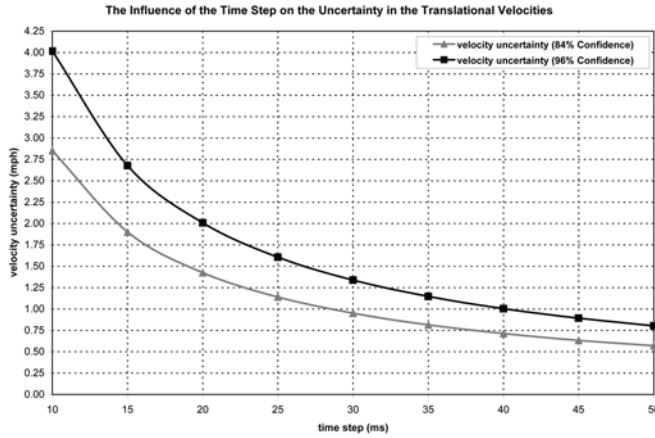


Figure 10 – Velocity Uncertainties

Figures 11 and 12 depict the vehicle’s translational speed and vertical speed for the first 2000 milliseconds of the test, calculated with Equations (2) and (3) and with time steps varying between 10 and 40 milliseconds.

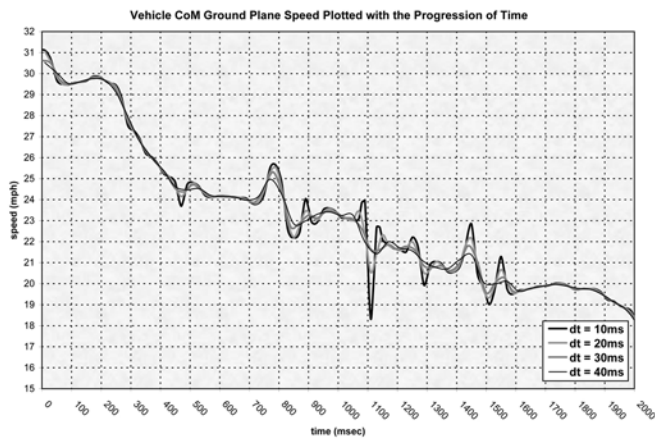


Figure 11 – Vehicle Translational Speed

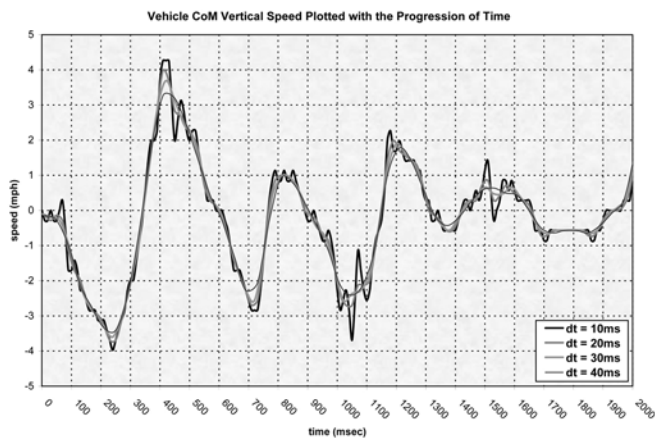


Figure 12 – Vehicle Vertical Speed

Examination of Figure 11 reveals that, with the exception of several small time segments, varying the time step between 10 and 40 milliseconds made little difference to the translational speed that was calculated with Equation (2). Examination of Figure 12 reveals that, for most time segments, varying the time step between 20 and 40 milliseconds made little difference to the vertical velocity that was calculated. At a time step of 10 milliseconds, the vertical velocity curve exhibits quite a bit of jumpiness that likely indicates this time step produces excessive sensitivity to measurement errors in the z-coordinate. In addition to this, the time step does have some effect on the peaks achieved by the vertical velocity curve, with the magnitude of the peaks being diminished as the time step increases.

Overall, for the velocity calculations, a time step of 40 milliseconds appeared to be a reasonable compromise between the effects of potential measurement errors and over-smoothing effects. This time step yielded an uncertainty in the translational velocities around 1 mph, with a confidence of 96%. Though the peaks of the vertical velocity curve with this time step may experience some truncation due to over-smoothing, this effect does not appear excessive.

Now, consider the vertical velocities of Figure 12 relative to what was physically occurring when the vehicle had these velocities. This graph shows that, as it exits the dolly and drops to the ground, the vehicle develops a downward velocity around 3-½ mph by the time the wheels impact the ground. As a result of the wheels impacting the ground, the vehicle then develops an upward velocity around 3-½ mph. The vehicle then falls again and at the time the leading side roof rail contact the ground the vehicle has a downward center of mass velocity around 2-½ mph. The upward velocity change from this first roof impact gives the vehicle an upward velocity of 1 mph. By the time the trailing side roof impact the ground, the vehicle has developed a downward velocity of around 2-½ mph. The vehicle rebounds out of this second roof contact with a vertical velocity around 2 mph.

After calculating the vehicle’s translational velocities, the following centered difference equation yielded the vehicle’s ground plane acceleration throughout the test:

$$a_x = \frac{v_{x,t+\Delta t} - v_{x,t-\Delta t}}{2\Delta t} \quad (6)$$

Similarly, the following difference equation yielded the vehicle’s vertical acceleration throughout the test:

$$a_z = \frac{v_{z,t+\Delta t} - v_{z,t-\Delta t}}{2\Delta t} \quad (7)$$

The following equation yielded the vehicle's resultant acceleration.

$$a_{res} = \sqrt{a_x^2 + a_z^2} \quad (8)$$

Figure 13 compares the resultant accelerations calculated with Equations (6) through (8), with varying time steps, to those obtained from sensor data. The sensor data was first filtered with a CFC 60 filter. With a time step of 20 milliseconds, Equations (6) through (8) appear to produce a rather erratic acceleration curve that potentially exhibits excessive noise due to measurement errors. However, at higher time steps the acceleration curves appear to be *potentially* subject to over-smoothing error since the peak of the accelerations are significantly influenced by the time step.

Any time step between 20 and 40 milliseconds yielded calculated peak accelerations that were significantly lower than those exhibited by the sensor data. Visually, the peaks of the sensor data appear to be influenced by considerable noise still present in the signals, and thus, it seems likely that the sensor signals in this case overestimate the peak accelerations. However, further analysis would be necessary to determine the degree to which the sensor signals might be overestimating the accelerations and, likewise, the degree to which the video analysis data might be underestimating the resultant accelerations.

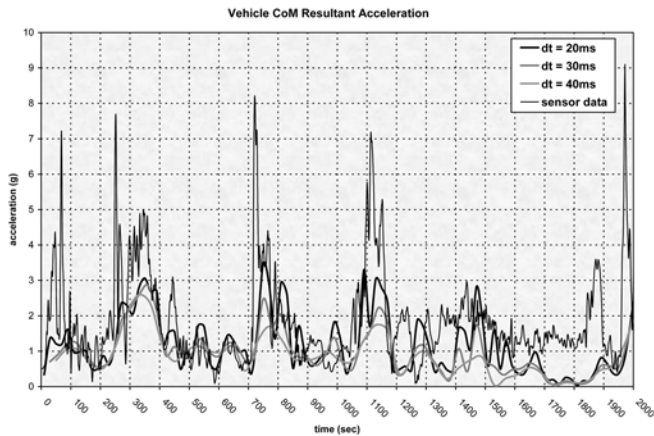


Figure 13 – Vehicle Resultant Accelerations

Using differential calculus to perform an error analysis on Equations (6) and (7), it can be shown that the uncertainty in the accelerations can be estimated with the following equations:

$$\delta a_x = \frac{\delta x}{2\Delta t^2} \quad (9)$$

$$\delta a_z = \frac{\delta z}{2\Delta t^2} \quad (10)$$

Again assuming that the differences between the two analysts reported above give a reasonable estimate of the potential measurement errors or the uncertainty in the positional coordinates obtained with the camera-matching technique, Figure 14 graphically represents Equations (9) and (10) for time steps varying between 10 and 50 milliseconds. From the standpoint of the uncertainty, using a time step of 40 milliseconds for calculating the accelerations yields an uncertainty in the translational accelerations of approximately 0.8g, with 96% confidence, and of approximately 0.57g with 84% confidence.

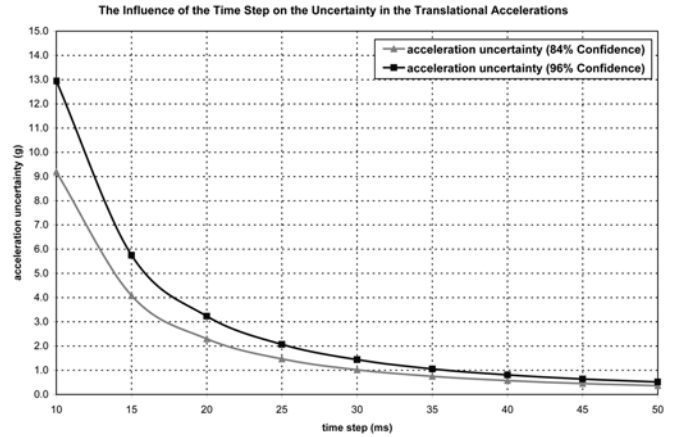


Figure 14 – Acceleration Uncertainties

Having calculated the test vehicle's CoM accelerations in the earth-fixed coordinate system, equations can be written relating these accelerations to the forces that caused them. To develop these equations, consider a free-body diagram for a vehicle whose roof is impacting the ground as shown in Figure 15.

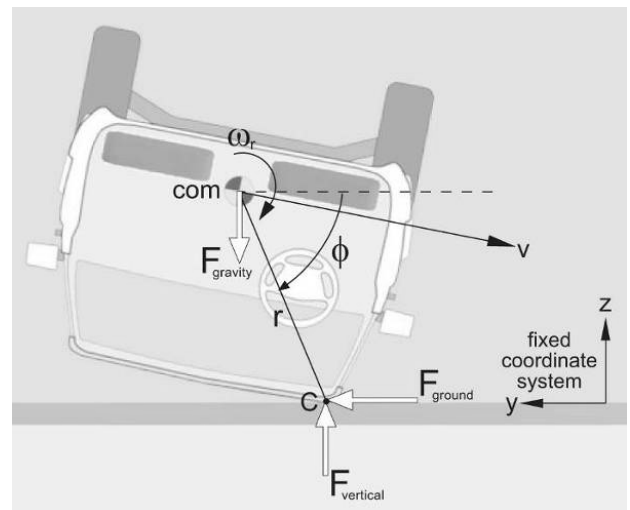


Figure 15 – Free-Body Diagram for a Vehicle-to-Ground Impact

This vehicle is depicted with a translational velocity both along and into the ground surface and with a roll velocity that contributes to the speed with which the roof impacts the ground. The geometry of this impact is described

with the parameters  $r$  and  $\phi$ , which will be referred to as the impact radius and the impact angle, respectively. The impact radius is the distance separating the center of mass and the contact area between the vehicle and the ground. The impact angle is the angle between the ground plane and the line connecting the center of mass to the vehicle's area of contact with the ground. During the impact depicted in Figure 15, the vehicle is subjected to a ground plane ( $F_{ground}$ ) and vertical component ( $F_{vertical}$ ) of the impact force and to the gravity force ( $F_{gravity}$ ), which is the vehicle weight.

The following equations describe the motion of this vehicle through the depicted impact:

$$ma_{cg,ground} = F_{ground} \quad (11)$$

$$ma_{cg,vertical} = F_{vertical} - F_{gravity} \quad (12)$$

$$I_{roll}\alpha_{roll} = F_{ground} \cdot r \cdot \sin\phi - F_{vertical} \cdot r \cdot \cos\phi \quad (13)$$

In these equations,  $m$  represents the vehicle's mass,  $I_{roll}$  represents its roll moment of inertia, and  $\alpha_{roll}$  represents its roll acceleration. These equations of motion provide a basis for interpreting the relationship between accelerations recorded at the vehicle's center-of-mass and the vehicle-to-ground impact forces to which the vehicle is subjected during a rollover crash test. The first two equations of motion can be rearranged, as follows, to reveal this interpretation:

$$\frac{F_{ground}}{W} = \frac{a_{cg,ground}}{g} \quad (14)$$

$$\frac{F_{vertical}}{W} = \frac{a_{cg,vertical}}{g} + 1 \quad (15)$$

Thus, the vehicle's center-of-mass acceleration along the ground surface, in gravitational units, can be interpreted as the vehicle-to-ground impact force along the ground surface, normalized by the vehicle weight. The vehicle's vertical center-of-gravity acceleration can be interpreted as a force that is 1g less than the vertical vehicle-to-ground impact force, normalized by the vehicle weight.

Figures 16 and 17 show the vertical impact force applied to the test vehicle during this test, calculated with Equation (15) and utilizing the accelerations calculated with time steps between 20 and 40 milliseconds. The first of these graphs plots the vertical force with the progression of time and the second plots the vertical force with the progression of the roll. In Figure 17, images have been included to show the orientation of the vehicle at the peak of each of three main impulses.

These three impulses are associated with the impact between the wheels and ground as the vehicle exits the dolly, the driver's side roof-to-ground impact, and the passenger side A-pillar, roof rail and hood impact with the ground.

The curves depicted in Figures 16 and 17 give us some ability to judge which time step produces the most accurate accelerations and forces. Physically, these force curves should not drop below zero, since the vertical impact force cannot be negative. However, both the 20 and 30 millisecond curves do drop significantly below zero over certain time intervals, and thus, they contain physically unrealistic values. With a time step of 40 milliseconds, these unrealistic negative impact force values are nearly eliminated. This gives one indication that the forces calculated with the 40 millisecond time interval are likely more accurate than those calculated with a 20 or 30 millisecond time interval. It is also likely an indication that the sensor accelerations of Figure 13 are overestimating the peak accelerations since these accelerations are directly related to the contact forces. Were these sensor accelerations used to calculate forces, they would no doubt produce peak forces well above those calculated with the video analysis at a time step of 40 milliseconds.

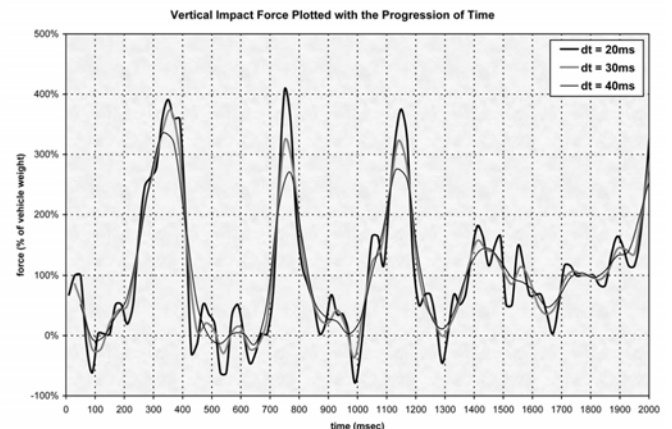


Figure 16 – Vertical Impact Force

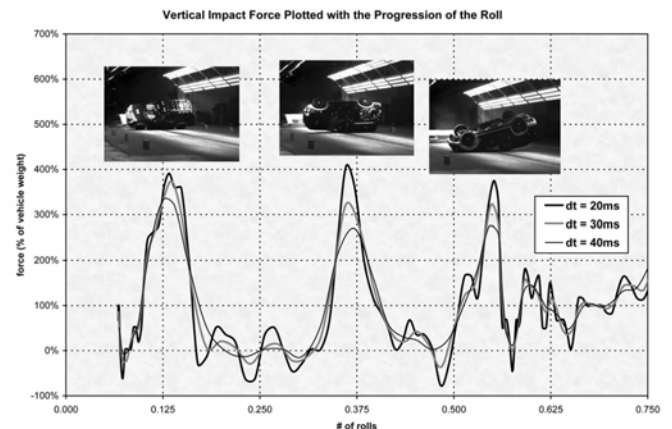


Figure 17 – Vertical Impact Force

On the other hand, review of the test video appears to show that using a 40 millisecond time step to calculate the vertical impact force results in impact durations that are too long. For instance, for the first wheel-to-ground impact, the 40ms force curve indicates the impact occurred over the time interval from 130 to 490 milliseconds. Review of the video reveals that this impact actually occurred over the interval of time from 220 to 450 milliseconds. Thus, the 40ms force curve implies an impact duration of 360ms for an impact that actually only lasted for approximately 230 milliseconds. In terms of the impact duration, then, the 20 and 30 millisecond force curves provide a better estimate of the overall impact durations.

Impact duration aside, given that the 40ms curve doesn't contain the physically unrealistic negative force values that the 20 and 30 ms curve do, the 40ms curve may still provide the most reasonable estimate of the peak impact forces. If that is the case, then the first wheel-to-ground impact produced a peak vertical impact force that was approximately 335% of the vehicle weight and both the driver's side and passenger's side roof impacts produced peak vertical impact forces of approximately 270% of the vehicle weight. That these vertical impact forces were able to be obtained from this crash test with relatively simple equations reveals a major advantage of obtaining the vehicle motion data from video analysis. Since the motion from that analysis is already resolved within the world coordinate system there is no need to transform the data from the vehicle coordinate system into the world coordinate system as would be necessary with the sensor data. Such transformation of the sensor data into the inertial reference frame is cumbersome and subject to potentially significant accrual of error.

Now, consider the vehicle's roll velocity. The following difference equation will yield the vehicle's average roll velocity over two time steps:

$$\omega_r = \frac{\theta_{r,t+\Delta t} - \theta_{r,t-\Delta t}}{2\Delta t} \quad (16)$$

In Equation (16),  $\theta_r$  is the vehicle roll angle at the specified time step. Similar equations could be written for obtaining the vehicle's pitch and yaw velocities.

Figure 18 compares the results from Equation (16), calculated with time steps between 10 and 40 milliseconds, with the roll velocity obtained from the two roll rate sensors on the vehicle. The sensor data shown in this graph was filtered with a CFC 60 filter. In general, the video analysis data and the sensor signals show acceptable agreement. In fact, the discrepancies between the sensor data and the video analysis were less significant than the discrepancies between the two sensors themselves. Overall, the agreement between the video analysis and the sensor data does not appear

significantly affected by the time step with which the roll velocity is calculated.

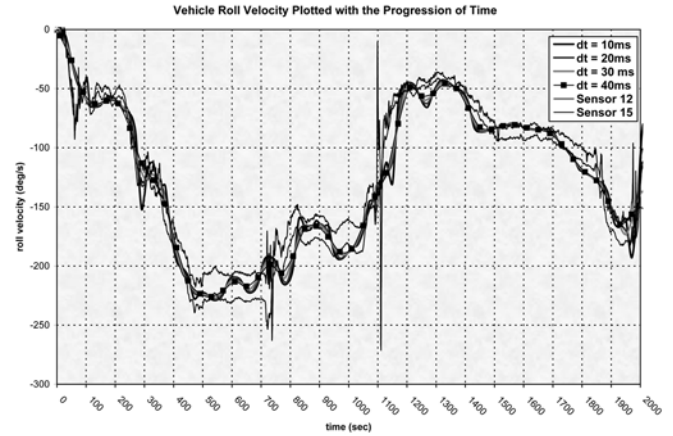


**Figure 18 – Vehicle Roll Velocity Curves**

Using differential calculus to perform an error analysis on Equations (16), it can be shown that the uncertainty in the roll velocity can be estimated with the following equation:

$$\delta\omega_r = \frac{\delta\theta_r}{\sqrt{2} \cdot \Delta t} \quad (17)$$

For the video analysis reported in this paper, it was found that when obtained by two separate analysts, the two set of motion data had an average difference in the roll angle of 0.58 degrees, with a standard deviation of 0.40 degrees. Thus, approximately 85% of the time, the difference between the roll angles obtained by the two analysts was less than 1 degree. Assuming that this average difference gives a reasonable estimate of the potential measurement errors or the uncertainty in the roll angles obtained with the camera-matching technique, Figure 19 graphically represents Equation (17) for time steps varying between 10 and 50 milliseconds.

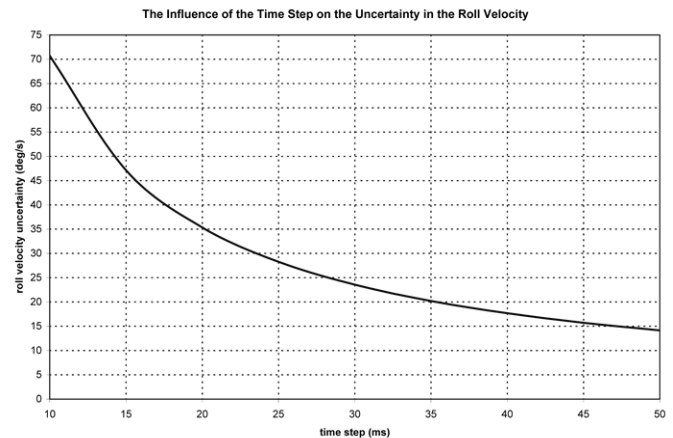


**Figure 19 – Roll Velocity Uncertainties**

Since the agreement between the roll velocities obtained with video analysis and the sensor data does not appear to depend significantly on the time step used to calculate the roll velocity, a 40 millisecond time step again seems a good choice for use in the video analysis calculations. At this time step, the uncertainty in the calculated roll velocities will be around 18 degrees per second, with a confidence of 85%.

Interestingly, the changes in roll velocity exhibited by the roll velocity curves of Figure 18 during each impact occurred over time intervals that were consistent with what the test video showed. That being the case, the roll velocity curves were used in conjunction with review of the video to obtain the time intervals over each of the three main impacts occurred. Those time intervals were as follows:

Impact #1 – 220 to 450 ms (230ms duration)

Impact #2 – 705 to 870 ms (165ms duration)

Impact #3 – 1030 to 1200 ms (170ms duration)

The following equation will yield the vehicle's energy at any instant in time during the test:

$$E = \frac{m}{2} \cdot (v_{x-y}^2 + v_z^2 + k_r^2 \omega_r^2 + k_p^2 \omega_p^2 + k_y^2 \omega_y^2) \quad (18)$$

In this equation,  $k_r$ ,  $k_p$  and  $k_y$  are the vehicle's radii of gyration and  $\omega_r$ ,  $\omega_p$  and  $\omega_y$  are the angular velocities. Figure 20 depicts the vehicle's kinetic energy for the first two seconds of the test.

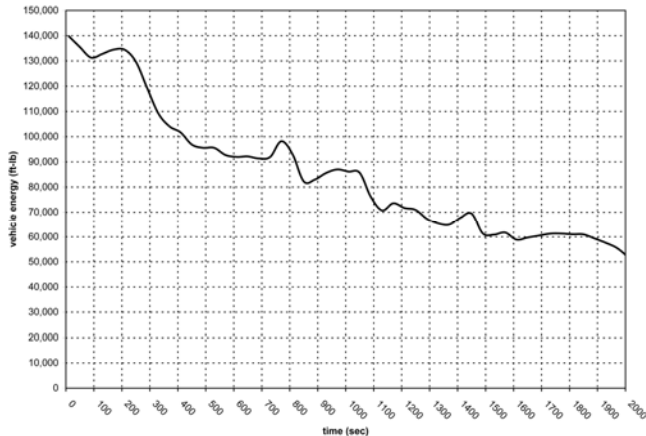


Figure 20 – Vehicle Energy

Using differential calculus to perform an error analysis on Equation (18), it can be shown that the uncertainty in the vehicle's kinetic energy can be estimated with the following equation:

$$\delta E = m \cdot \sqrt{v_{x-y}^2 \delta v_{x-y}^2 + v_z^2 \delta v_z^2 + k_r^4 \omega_r^2 \delta \omega_r^2 + k_p^4 \omega_p^2 \delta \omega_p^2 + k_y^4 \omega_y^2 \delta \omega_y^2} \quad (19)$$

In this equation,  $\delta \omega_r$ ,  $\delta \omega_p$ , and  $\delta \omega_y$  are the angular velocity uncertainties. The energy loss for each of the three main impacts that occurred during this test can be obtained by subtracting the vehicle's kinetic energy at the end of the impact from its kinetic energy at the beginning of impact. Using differential calculus to determine the uncertainty in these energy losses, following equation is obtained:

$$\delta \Delta E = \sqrt{\delta E_f^2 + \delta E_i^2} \quad (20)$$

In this equation,  $\delta \Delta E$  is the overall uncertainty in the calculated energy loss,  $\delta E_f$  is the uncertainty in the vehicle's calculated energy loss at the end of the impact, and  $\delta E_i$  is the uncertainty in the vehicle's calculated energy loss at the beginning of the impact.

Given the impact time intervals reported above, the data of Figure 20 can be used to obtain the following energy losses for each of the three main impacts:

$$\Delta E_1 = 36,371 \text{ ft-lbs} \pm 8,219 \text{ ft-lbs} (27.3\% \pm 6.2\%)$$

$$\Delta E_2 = 8,957 \text{ ft-lbs} \pm 7,262 \text{ ft-lbs} (9.8\% \pm 7.9\%)$$

$$\Delta E_3 = 13,749 \text{ ft-lbs} \pm 6,932 \text{ ft-lbs} (16.0\% \pm 8.1\%)$$

The uncertainties reported with the above energy losses have a confidence of approximately 85%. These uncertainties are rather significant relative to the best estimate values. Clearly, considerable uncertainty has accrued through the course of the calculations carried out in this paper.

## QUANTIFYING DEFORMATION TO THE A-PILLARS

The motion of the vehicle in the rollover test was tracked using a high polygonal mesh computer model that was identical in size, shape and form to the vehicle in the test. Because this polygonal mesh model is finely detailed and contains a tight matrix of data points in the areas of the roof frame and A-pillar, it was possible to estimate the deformation to the vehicle's A-pillars during the roof's impacts with the ground. There were two distinct impacts between the vehicle's roof and the ground, one on the driver's side and one on the passenger's side. For each of these impacts, the dynamic deformation of the engaged A-pillar was estimated.

To quantify the deformation of the engaged A-pillar during each impact, a point on the corner of the A-pillar

and roof frame was chosen on the high polygonal mesh model that was also surveyed on the test vehicle prior to the rollover test initiation. Figure 21 shows this point for the passenger side A-pillar as a fiducial sticker placed on the test vehicle.



**Figure 21 – Fiducial Sticker on Passenger’s Side A-Pillar Used for Deformation Measurement**

This same point was identified on the mesh model in a camera match of a close up view of the impact recorded by one of the high speed cameras set up for this specific purpose. Since the ground plane itself was surveyed, and the high polygonal mesh model matched the motion seen in the video, the distance that a point on the A-pillar traveled past this ground plane could be determined. In other words, if that point is treated as a rigid connection to the rest of the vehicle, the distance that point on the model penetrated the ground plane in the camera view was considered to be the amount of deformation. This distance is calculated as the perpendicular difference between the point on the A-pillar and the ground plane, the largest distance at any frame marking the vehicles maximum deformation. Figure 22 graphically depicts the manner in which the deformation measurements were taken.

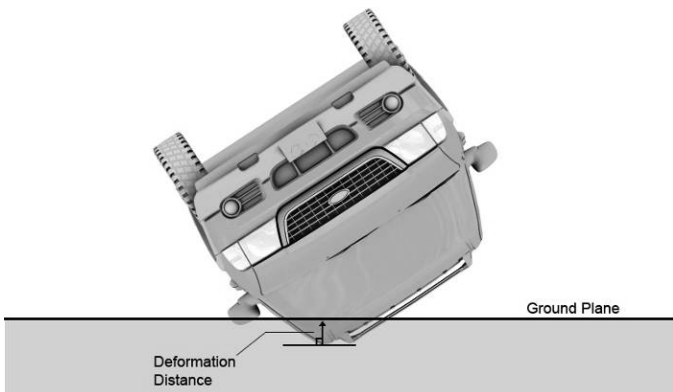


**Figure 22 – Deformation Measurement Methodology**

Clearly, this definition of the deformation has limitations. For instance, deformation of the roof due to the ground

plane force is neglected. The reason for employing this specific method of estimating the deformation is taken up in the “Discussion” section. In that section, suggestions are also made for improving this technique in future testing.

Figure 23 shows the estimated deformation distance for the driver’s side A-pillar during the first roof-to-ground impact. Figure 24 shows the estimated deformation distance of the passenger’s side A-pillar during the second roof-to-ground impact.



**Figure 23 – Driver’s A-Pillar Deformation**

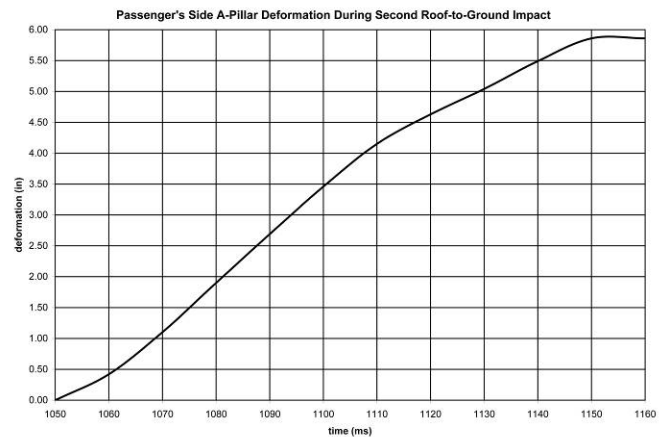


**Figure 24 – Passenger’s A-Pillar Deformation**

## DISCUSSION

This paper has examined the use of a camera-matching video analysis technique to quantify the vehicle dynamics and deformation for a dolly rollover test run in accordance with the SAE Recommended Practice J2114. The subsections that follow consider the viability of this technique for these purposes.

## Vehicle Dynamics

The camera-matching technique described in this paper was used to obtain whole-body kinematics for the test

vehicle. Once these kinematics were obtained. Equations (1), (2), (3), (6), (7), (8) and (16) provided motion analysis equations for processing this kinematics data. Equations (14) and (15) provided equations for obtaining the components of the impact forces from the kinematics data. In general, the accuracy and precision of the parameters calculated with these equations will depend on the magnitude of the measurement error in the positional coordinates and on the time step used for the calculation. On the one hand, if too small a time step is used, the velocity calculations will be excessively sensitive to any measurement errors and will exhibit excessive uncertainty. On the other hand, if too large a time step is used, the velocity curves will suffer from over-smoothing error and the velocity peaks could be truncated.

Overall, for the test considered here, it was found that a time step of 40 milliseconds minimized the effects of measurement error while at the same time producing realistic impact force values. Smaller time steps were associated with excessive uncertainty and with physically unrealistic negative impact force values. The peak accelerations calculated from the video analysis data with a 40 millisecond time step were significantly lower than those exhibited by the sensor data. Visually, the peaks of the sensor data appear to be influenced by considerable noise still present in the signals, and thus, it seems likely that the sensor signals in this case overestimated the peak accelerations. More aggressive filtering of the sensor data could perhaps resolve this discrepancy.

That the vertical impact forces were able to be obtained from this crash test with relatively simple equations reveals a major advantage of obtaining the vehicle motion data from video analysis. Since the motion from that analysis is already resolved within the world coordinate system there is no need to transform the data from the vehicle coordinate system into the world coordinate system as would be necessary with the sensor data. Such transformation of the sensor data into the inertial reference frame is cumbersome and subject to potentially significant accrual of error.

## **Deformation**

A difficulty that arises in using any type of motion tracking method to obtain the motion of a vehicle during a rollover test is the fact that the vehicle deforms throughout the test. As the vehicle experiences that deformation, the pre-test positions of points on the vehicle change relative to one another. While an automated motion-tracking system could be used to track the motion of specific points on the vehicle during a rollover test, without being able to resolve the degree to which those points move relative to one another due to deformation, one would not be able to relate the motion

of these points to the whole-body kinematics of the vehicle.

The manual, model-based motion tracking scheme used in this paper did resolve this to some degree since, at any given time in the video, the analyst could use portions of the vehicle that, in their judgment, were not deforming to achieve the best match with the overall vehicle motion. This worked well for the test analyzed in this paper since the vehicle only rolled one time. In applying this method to a test in which the vehicle rolled more than one time, one would likely encounter similar difficulties to those that would be encountered in trying to extract whole-body motion from points tracked with an automated tracking scheme. To parse out the separate deformations for each impact, the analyst would need to create a new computer model of the vehicle after each roll that incorporated the deformation for that roll. This process would be cumbersome since creation of the intermediate damaged vehicle model would depend on the use of photogrammetry techniques. Determining the viability of such a technique would require more research.

In the previous section, deformation data was reported for the top of the driver's side A-pillar during the first roof-to-ground impact and for the top of the passenger's side A-pillar during the second roof-to-ground impact. These deformations were calculated by determining the distance that a point on the A-pillar of our vehicle computer model traveled past the ground plane during the impact. In other words, this point was treated as a rigid connection to the rest of the vehicle and the distance this point penetrated the ground plane, measured perpendicular to the ground, was considered to be the amount of deformation.

McClenathan, et al., [6] have observed that current methods of measuring the time history of deformation during a crash test "are limited by the use of electro-mechanical devices such as string pots and/or linear variable displacement transducers (LVDT). Typically, one end of the transducer must be mounted to a point on the structure that will remain un-deformed during the event; the other end is then attached to the point on the structure where the deformation is to be measured. This approach measures the change in distance between these two points and is unable to resolve any movement into its respective X, Y, or Z directions."

The technique used here in this paper to measure the deformation of the vehicle at the A-pillars, using off-board cameras, shares this same inability to resolve the three-dimensional character of this deformation. The difficulty in obtaining such three-dimensional deformation data from the technique employed in this paper relates almost entirely to the fact that the deforming components are not visible in the video footage being analyzed. Instead, the analyst must infer the deformation based on

the position of the portions of the vehicle that is visible in the video.

McClenathan was able to obtain three-dimensional deformation data using a motion-tracking technique and video from interior, on-board video footage. In this case, the deforming structures were visible in the video. There will generally be a discrepancy between the deformation of interior structures and the external deformation of the vehicle. It may be that the fullest resolution of the time history of deformation associated with a particular roof-to-ground impact would result from combining analysis of on-board and off-board video footage with data from some sort of electro-mechanical device for measuring deformation. The on-board video footage and the data from a transducer would allow the analyst to see aspects of the deformation that are not visible in the off-board video footage.

## CONCLUSIONS

1. Overall, vehicle motion data obtained by two different analysts had an average difference in the x-coordinate of 0.35 inches, an average difference in the z-coordinate of 0.42 inches, and an average difference in the roll angle of 0.58 degrees.
2. Overall, for the test considered here, it was found that a time step of 40 milliseconds minimized the effects of measurement error while at the same time producing realistic impact force values. Smaller time steps were associated with excessive uncertainty and with physically unrealistic negative impact force values.
3. The peak accelerations calculated from the video analysis data with a 40 millisecond time step were significantly lower than those exhibited by the sensor data. Visually, the peaks of the sensor data appear to be influenced by considerable noise still present in the signals, and thus, it seems likely that the sensor signals in this case overestimated the peak accelerations. More aggressive filtering of the sensor data could perhaps resolve this discrepancy.
4. A time step of 40 milliseconds yielded an uncertainty in the translational velocities that was less than ½ mph and an uncertainty in the roll velocities that was approximately 10 degrees per second.
5. There was acceptable agreement between the roll velocity data obtained from the video analysis and that obtained from sensors. In fact, the discrepancies that existed between the sensor data and the video analysis were of less significance than the discrepancies between the two sensors themselves.

6. Deformation data was reported for the top of the driver's side A-pillar during the first roof-to-ground impact and for the top of the passenger's side A-pillar during the second roof-to-ground impact. However, the deforming structures were not visible in the test video, and so, the deformation was inferred from the motion of those portions of the vehicle that were visible. Since the deformation was inferred, it could not be fully resolved in three-dimensions, and in fact, the method used to infer it assumed that the ground surface impact force caused no deformation.
7. The fullest resolution of the time history of deformation associated with a particular roof-to-ground impact could potentially result from combining analysis of on-board and off-board video footage with data from some sort of electro-mechanical device for measuring deformation. The on-board video footage and the data from a transducer would allow the analyst to see aspects of the deformation that are not visible in the off-board video footage. Further research could explore such an approach for obtaining a time history of deformation.

## REFERENCES

1. Chou, Clifford C., McCoy, Robert W., Le, Jerry Jialiang, Fenton, Stephen J., Neale, William T.C., Rose, Nathan A., "Image Analysis of Rollover Crash Tests Using Photogrammetry," Society of Automotive Engineers (SAE) Technical Paper Number 2006-01-0723.
2. Chou, Clifford C., McCoy, Robert W., Le, Jialiang, "A Literature Review of Rollover Test Methodologies," *Int. J. Vehicle Safety*, Volume 1, Nos. 1/2/3, 2005.
3. "Dolly Rollover Recommended Test Procedure," Surface Vehicle Recommended Practice J2114, Society of Automotive Engineers, October 1999.
4. Harper, David G., Blake, Robert W., "A Critical Analysis of the Use of High-Speed Film to Determine Maximum Accelerations of Fish," *J. exp. Biol.*, 142, 465-471 (1989).
5. Hoffman, Joe D., "Numerical Methods for Engineers and Scientists," Second Edition, Marcel Dekker, 2001.
6. McClenathan, Robert V., Nakhla, Said S., McCoy, Robert W., Chou, Clifford C., "Use of Photogrammetry in Extracting 3D Structural Deformation/Dummy Occupant Movement Time History During Vehicle Crashes," SAE Technical Paper Number 2005-01-0740.

7. Seitz, Thomas, Bubb, Heiner, "Human-Model Based Movement-Capturing Without Markers for Ergonomic Studies," SAE Technical Paper Number 2001-01-2113.
8. Taylor, John R., An Introduction to Error Analysis, Second Edition, University Science Books, 1997.